Int. J. Heat Mass Transfer. Vol. 36, No. 16, pp. 3887–3895, 1993
Printed in Great Britain

0017–9310/93 $6.00 + 0.00

The overall thermal conductivity in a straining body with microcrack evolution

DA YU TZOU and JING LI

Department of Mechanical Engineering, The University of New Mexico, Albuquerque, NM 87131, U.S.A.

(*Received* 23 *June* 1992 *and in final form* 10 *May* 1993)

Abstract—The overall thermal conductivity in a cracked solid with microcracks evolving in the strain history is studied in this work. The strain field aggravated by the increase of microcrack density and its effect on the overall degradation of thermal conductivity is illustrated. Special emphases are placed on the deformation-induced inhomogeneity and the path-dependency resulting from the evolution of microcracks. The micro-mechanical model established by Budiansky and O'Connell for the degradation of elastic moduli and that established by Tzou for the degradation of overall thermal conductivity are bridged together to describe this complicated phenomenon.

INTRODUCTION

MICROVOIDS or microcracks in solids are internal structures which reduce the effective surface area carrying thermal energy or mechanical load. Degradation of the load- or energy-bearing capacities of the solid, consequently, depends on the total amount of surface reduction when new pores or microcracks are initiated or existing defects are enlarged or lengthened in a strain history. The total volume occupied by such defects in the entire body has been identified to describe the group behavior of microcracks [1–3]. For geological materials such as rocks or concretes, the microcracks or voids result from natural consequences. They slowly evolve through months or years in service and degradations of thermal conductivity or elastic moduli at a certain instant can be calculated based upon a fixed value of the microcrack density. For ceramics, powder metallurgy materials, or solder joints in electronic packaging, on the other hand, the microcracks resulting from either manufacturing processs or weaker structural integrity may evolve with straining in a shorter period of time. The thermally-induced strain in solder joints subjecting to fatigue cycles spanned in the high range of homologous temperature [4], for example, promotes evolution of microcracks. The microcrack density increasing from one cycle to another not only degrades the overall moduli and consequently aggravates the shear localization, but also reduces the overall thermal conductivity which is responsible for the temperature localization. These two failure modes significantly reduce the lifetime performance of solder joints and consistently damage the electronic devices. For concretes under either tension or compression, the accumulative damage model developed by Tzou and Chen [5] provides another example for microcrack evolutions. The microcrack density has been found to dramatically increase in the post-peak softening range. As a result, the process zone spreads widely out of the near-tip region and becomes non-local.

Weakening of the energy-carrying capacity of the solid due to microcracks is reflected by degradations of the thermal conductivity. For the overall elastic moduli in cracked or composite bodies with multiple constituents, the famous self-consistent approach initiated by Budiansky [1, 2] and Budiansky and O'Connell [3] is the first attempt in resolving the microcracking damage. The approach was advanced later by Horii and Nemat-Nasser [6] to account for the anisotropic response due to friction in crack-closing. Their effort makes the self-consistent method more rigorous and systematic for studying the effects of internal cracks. The lumped formulation employing the self-consistent concept is also extended to study the overall thermal conductivity in cracked solids [7, 8]. The differential formulation reflecting the refined structure of microcracks was accomplished by Tzou [9, 10] which isolates the microcracking effect in an added tensor from the overall thermal conductivity tensor. A thorough comparison with the existing models [1, 11, 12] and experimental results [13, 14] is made to validate the model in general. The central quantity in the model is the temperature distribution around the crack (or pore) surfaces. When extended to a more complicated environment, dependency of the overall thermal conductivity on the Biot number simply cannot be described by the other models. It has been shown that when energy exchange between the matrix material and the internal cavities takes place, the overall thermal conductivity is a nonlinear function of the microcrack density.

Microcracks may evolve when a solid is strained. As a result, the overall thermal conductivity depending on the microcrack density varies in a strain history. For degradations of elastic moduli in the strain history and the resulting damage of shear locations, the research is in the broad area of brittle damage mech-

NOMENCLATURE

a	averaged radius of microcracks [mm]
C_d	microcrack density parameter [dimensionless]
D	microcrack damage index [dimensionless]
E	Young's modulus [MPa]
k	damage parameter [dimensionless]
K	bulk modulus [MPa]
N	number of activated cracks per unit volume.

Greek letters

β	shape factor of microcracks [dimensionless]
ε	uniaxial strain [mm mm^{-1}]
κ	thermal conductivity [W m^{-1} K^{-1}]
ν	Poisson's ratio
σ	uniaxial stress [MPa].

Subscripts and superscripts

0	intact values
v	volumetric quantities.

anics. It is still an ongoing research area and intensive reviews on the development of the theory have been frequently made [15, 16]. In companion with the degradation of elastic moduli due to microcracking, degradation of thermal conductivity may significantly increase the temperature established in the solid. This phenomenon becomes pronounced in solids containing localized defects such as a macrocrack tip or a notch. Due to large volumetric strain developed in the neighborhood of a macroscopic crack tip, for example, the number density of microcracks dramatically increases in the strain history. The resulting degradation of thermal conductivity in this local area prevents heat from dissipating into the surrounding media and localization of temperature occurs. Obviously, the thermo-mechanical interactions involved in this process may significantly influence the crack instability as well as the evolution of the process zone.

The present paper aims to study the overall thermal conductivity in a solid with evolving microcracks. At the initial stage of development, an uncoupled approach will be adopted which estimates the microcrack damage without incorporating the thermal effect. The micro-mechanical model established by Budiansky and O'Connell [3] and the microcracking damage model established by Tzou and Chen [5] are bridged together to depict the evolution of microcracks in the strain history. The microcrack density thus obtained will then be used to estimate the overall thermal conductivity according to the self-consistent result obtained by Tzou [9, 10]. The one-dimensional example is used to illustrate the essence of the model which includes the path-dependency of the overall thermal conductivity on strains. A general application is then made for a hollow cylinder subjected to internal pressure. The purpose is to obtain the evolution pattern of the overall thermal conductivity in the strain history and illuminate the inhomogeneity induced by deformation. It will be shown that the self-consistent approach results in an ultimate value of one-half (1/2) for the overall thermal conductivity relative to its intact value while the load-bearing capacity of the solid is totally lost. It shows that the energy-bearing capacity degrades at a *slower* rate than the load-bearing capacity in a nonisothermal environment.

MICROCRACK DAMAGE

Since the overall thermal conductivity sensitively varies with the microcrack density, it is necessary to describe the physical mechanisms governing the evolution of microcracks in a straining body. The stress intensity factor, first of all, is not a reliable index for measuring the crack damage when crack sizes are small [17, 18]. Especially for solids containing hundreds and thousands of such microcracks, emphasis should be placed on the *group* behavior rather than individual cracks. The microcrack density parameter measuring the averaged volume of randomly distributed microcracks,

$$C_d = \beta N a^3, \tag{1}$$

was used for this purpose [3]. In equation (1), C_d is the microcrack density parameter, N the number of cracks per unit volume, and a the average crack length. β is the shape factor depending on the geometry of microcracks. For circular cracks, the value of β is one (1). The microcrack density parameter (C_d) is promoted by either crack-lengthening (a increases) or activation of new cracks (N increases).

(a) *Overall elastic moduli*

Assuming that crack closure effects are negligible and the statistical distributions of the lengths, locations and orientations of the cracks are sufficiently random and uncorrelated (which implies that the cracks are non-interacting), Budiansky and O'Connell [3] derived the overall value for the elastic bulk modulus:

$$\frac{K}{K_0} = 1 - \frac{16}{9}\left(\frac{1-\nu^2}{1-2\nu}\right)C_d \tag{2}$$

with K being the bulk modulus and ν Poisson's ratio. The subscript '0' in this paper denotes the intact value. In relation to the degraded value of Poisson's ratio, the crack density parameter is further expressed as

$$C_d = \frac{45}{16}\frac{(\nu_0-\nu)(2-\nu)}{(1-\nu^2)[10\nu_0-\nu(1+3\nu_0)]}. \tag{3}$$

Note that under the assumptions made in the self-consistent approach, the cracked body characterized

by (2) and (3) behaves isotropically and homogeneously in the large. The degraded Poisson ratio, refer to equation (3), is a function of the crack density parameter. The degraded bulk modulus depicted by equation (2), consequently, varies with the crack density parameter in a nonlinear fashion.

(b) *Overall thermal conductivity*

The overall thermal conductivity has been derived by Tzou [9, 10] based on the same self-consistent concept,

$$\frac{\kappa}{\kappa_0} = 1 - \tfrac{8}{9} C_d \tag{4}$$

with κ being the thermal conductivity. The coefficient in front of C_d depends on the shape of defects. For microvoids with a spherical geometry, the coefficient 8/9 in equation (4) is replaced by $2\pi/3$. Larger degradation results for spherical pores than penny-shaped cracks because spherical pores, once activated, reduce more surface area carrying the thermal energy. In comparison with the corresponding expression for the elastic bulk modulus, equation (2), the constant coefficient (8/9) is much simpler due to the absence of lateral effect (parallel to Poisson's effect in solid deformation) in heat conduction. Most importantly, the overall thermal conductivity varies linearly with the crack density parameter when the lateral effect disappears. This is only valid, however, for insulated crack surfaces. In the presence of internal heat transfer across the surfaces of defects, the overall thermal conductivity becomes a nonlinear function of the crack density parameter. It involves the Biot number for a convective-mode heat transfer and the ratio of thermal conductivities of the primary to the secondary phase constituents for a conduction-mode heat transfer.

(c) *Deformation mechanisms*

The crack density parameter C_d appears as an independent variable in equations (2)–(4). For a *rigid* solid with a fixed structure of microcracks, C_d has a specific value and these equations can be used to calculate the overall values of K, ν, and κ. For a *deformable* body in which microcrack density evolves in straining, on the other hand, the relationship between microcrack density and strain must be established to describe the degradation process. The physical mechanism is thus controlled by strain in a loading history. From a physical point of view, the volume change of a material continuum (at least as a first-order approximation) is governed by the volumetric strain. The volumetric strain is defined as the sum of three principal strain components which reduces to the uniaxial strain in simple tension or compression. Recognizing that volume expansion is the major cause of microcrack activations, Tzou and Chen [5] extended this concept to their cumulative damage model. The index D measuring the microcrack damage,

$$D = \frac{16}{9}\left(\frac{1-\nu^2}{1-2\nu}\right) C_d, \tag{5}$$

was introduced for this purpose. In terms of D, equation (2) becomes

$$\frac{K}{K_0} = 1 - D. \tag{6}$$

In the absence of microcracks, the crack density parameter $C_d = 0$ which results in $D = 0$ from equation (5). The overall bulk modulus thus reduces to its intact value according to equation (6). In severe damage situations with D being one (1), $K = 0$ and the load-bearing capacity in the local area is totally lost. At specific values of C_d and ν_0, equation (3) provides a cubic equation to be solved for ν. A first-order Taylor series expansion on ν/ν_0 applied to (3), however, gives

$$\frac{\nu}{\nu_0} \simeq \frac{10}{9+2\nu}\left(1 - \frac{16}{9} C_d\right). \tag{7}$$

For typical values of ν ranging from 0 to 0.5 (for an incompressible medium) in the damage process, this ratio can be further approximated by

$$\nu \simeq \nu_0\left(1 - \frac{16}{9} C_d\right). \tag{8}$$

Numerically, as also demonstrated by a direct comparison of (3) and (8) for various values of ν [19], the maximum deviation between equations (3) (exact) and (7) (approximate) is 6.61%. The physical mechanisms behind equation (3), however, are better represented by equation (8). When the crack density parameter C_d reaches a limit value of 9/16 (0.5652), ν degrades to its final value of zero (0). This is an exact result should equation (3) be used. From equation (5), moreover, the damage D increases to its ultimate value of one (1) and the overall bulk modulus K reduces to zero (0) according to equation (6). In other words, total loss of load-carrying capacity occurs at $C_d = 9/16$. This critical instant does not have to wait until microcracks fill the entire solid. A detailed analysis to equation (5) further supports this observation. Solving equation (5) for ν, we obtain

$$\nu = \frac{9D - \sqrt{(81D^2 - 144DC_d + 256C_d^2)}}{16C_d}. \tag{9}$$

For $D = 1$ and $C_d = 9/16$, clearly, ν reduces to zero and the critical condition is thus retrieved. Equations (8) and (9) can be solved simultaneously for C_d and ν in terms of ν_0 and D. Equating (8) to (9), we arrive at a cubic equation governing C_d:

$$\left(\frac{4096\nu_0^2}{729}\right) C_d^3 - \left(\frac{512\nu_0^2}{81}\right) C_d^2 + \left[\frac{16(\nu_0^2 + 2D\nu_0 - 1)}{9}\right] C_d + D(1 - 2\nu_0) = 0. \tag{10}$$

Again, the condition of $D = 1$ when $C_d = 9/16$ is

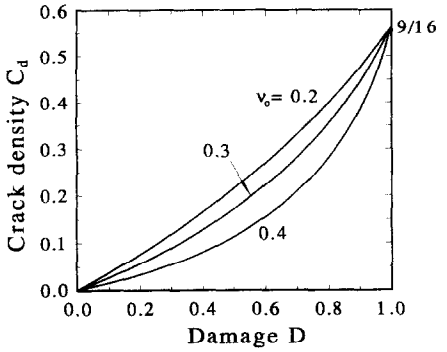

FIG. 1. Variations of the microcrack density parameter (C_d) with the intact Poisson's ratio (v_0) and the microcrack damage measure (D).

reflected. In a deformation history with D being determined, therefore, the crack density parameter (from (10)) and the degraded Poisson's ratio (from (8) or (9)) can be obtained altogether. Figures 1 and 2 show the variations of C_d and v with v_0 and D. Although analytical solutions for the cubic equation (10) exist, the secant method is used for these figures. The procedure is straightforward since the root for C_d is between zero and 9/16 for all cases. As shown in Fig. 1, the crack density parameter increases to its ultimate value of 9/16 when the damage increases to one. At a certain value of D developed in the strain history, more microcracks (larger value of C_d) are activated in the solid with a smaller value of the intact Poisson's ratio (v_0). Figure 2 shows the degradation of Poisson's ratio when the microcrack damage increases. For various values of v_0, the overall Poisson's ratio degrades to zero when severe damage ($D = 1$) occurs.

Phenomenologically, the microcrack density (C_d) and hence the microcrack damage (D) increase when the volumetric strain in a material continuum increases. This behavior has been described in the micro-mechanical models in continuum damage mechanics. The model established by Tzou and Chen [5] provides a typical example. Employing the Weibull distribution for the number of active flaws per unit volume and relating the averaged radius of the circular cracks to the volumetric strain and the critical stress intensity factor, they obtained

$$D = k\varepsilon_v^{m-6} \tag{11}$$

where ε_v is the volumetric strain measuring the volume change of a material continuum in small deformations. k and m are the damage parameters determined from the peak-state of softening damage in the uniaxial stress–strain curve. From the experimental curves of concretes, their values were found as

$$k = 1.05311 \times 10^6, \quad m = 7.88917 \quad \text{under tension,}$$
$$k = 1.51523 \times 10^8, \quad m = 9.52216 \quad \text{under compression.} \tag{12}$$

Since tension and compression possess different values of k and m, the damage model is capable of distinguishing tensile and compressive damage. In a uniaxial response, the volumetric strain reduces to the uniaxial strain. The uniaxial stress–strain curve is thus described by

$$\sigma = E_0(1-D)\varepsilon = E_0(\varepsilon - k\varepsilon^{m-5}) \tag{13}$$

where E_0 is the intact value of Young's modulus. For the same concrete specimen, $E_0 = 21\,390$ MPa under tension and 20 576 MPa under compression. The intact Poisson's ratio, however, is not sensitive to the loading condition and remains at 0.24 for both cases. The post-peak softening behavior represented by equation (13) is shown by Fig. 3 for both tension and compression. In companion with the strain increase, microcracks activate in the post-peak region and the stress already established in the medium relaxes due to formation of new crack surfaces.

Note that for describing the overall degradation of thermal conductivity in a strain history, the constitutive equation (13) must be accommodated to address the effect of microcracking in a consistent fashion. Traditional approaches employing elasticity or plasticity theory for describing deformations, therefore, are limited to the physical domain in which

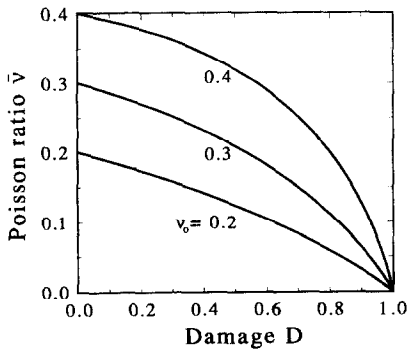

FIG. 2. Variations of the degraded Poisson's ratio (v) with the intact Poisson's ratio (v_0) and the microcrack damage measure (D).

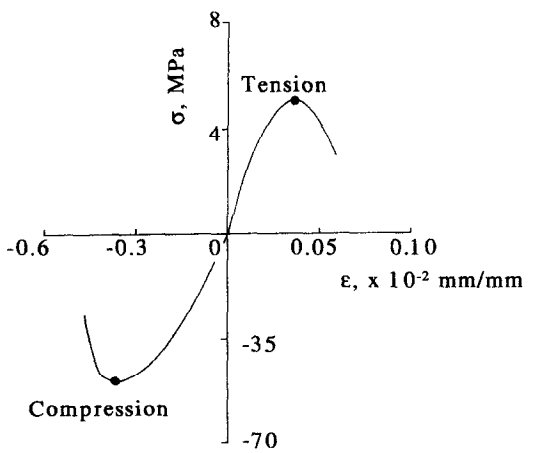

FIG. 3. The post-peak softening damage of a concrete specimen under tension and compression.

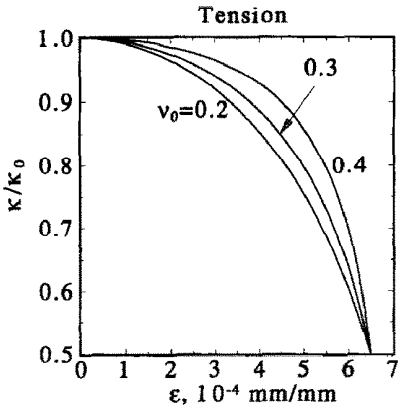

FIG. 4. Degradation of the overall thermal conductivity in the strain history. The concrete specimen under tension, $k = 1.05311 \times 10^6$ and $m = 7.88917$.

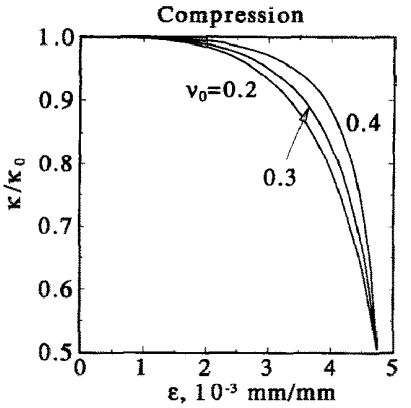

FIG. 5. Degradation of the overall thermal conductivity in the strain history. The concrete specimen under compression, $k = 1.51523 \times 10^8$ and $m = 9.52216$.

microcracks are not activated. Consequently, the microcrack density cannot be high. On the contrary, the present model accommodates degradations of the overall elastic moduli as an entirety when microcrack density increases. As a result, the model is expected to cover a wider range of microcrack density evolving the strain history.

OVERALL THERMAL CONDUCTIVITY

The load-bearing capacity of the continuum volume will be totally lost when C_d reaches a value of 9/16. Both the bulk modulus and Poisson ratio degrade to zero at this critical instant. The conductivity ratio κ/κ_0, on the other hand, degrades to an ultimate value of one-half (1/2) according to equation (4). The continuum elements with 'saturated' microcracks (when $C_d = 9/16$) can still conduct heat but not as efficiently. Clearly, the load-bearing capacity of a material volume due to microcracking degrades at a *faster* rate than the energy-bearing capacity.

(a) *One-dimensional response*

So far, equations (4) relating the overall thermal conductivity to the microcrack density parameter, (10) relating the microcrack density parameter to the microcrack damage, and (11) relating the microcrack damage to the volumetric strain are available for use. Combinations of equations (4), (10) and (11), therefore, gives us an expression for the overall thermal conductivity evolving with the microcracks in the strain history:

$$\frac{\kappa}{\kappa_0} = 1 - \tfrac{8}{9} C_d(D(\varepsilon); \nu_0, k, m). \tag{14}$$

Different values of k and m should be used when the loading switches from tension to compression. For various values of ν_0, Figs. 4 and 5 show the variations of the overall thermal conductivity in the strain history. When the strain increases to approximately 6.48×10^{-4} mm mm^{-1} in tension and 4.75×10^{-3} mm mm^{-1} in compression, the overall thermal conductivity ratio degrades to its ultimate value of 0.5. With regard to the energy-bearing capacity, clearly, the specimen has stronger resistance to compression. This behavior is consistent with that in deformation because microcracks are less activated under *overall* compression than those under tension.† Degradation of the overall thermal conductivity can also be presented in terms of the stress according to equation (12). The results are displayed in Figs. 6 (for tension) and 7 (for compression). Both figures start from the right where the overall thermal conductivity degrades from its intact value. It is clear that most degradations occur in the post-peak region after softening. The analysis based on the elastic response without incorporating microcrack damage, therefore, is limited to the domain prior to the softening point. It can only predict, approximately, 10% of the degradation in tension ($\kappa/\kappa_0 \simeq 0.9$) and 5% in compression ($\kappa/\kappa_0 \simeq 0.95$). Any degradation beyond this threshold must accommodate the softening damage in the mechanical response for the sake of consistency.

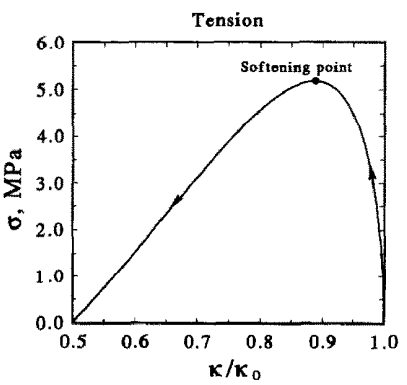

FIG. 6. Degradation of the overall thermal conductivity in the stress history. The concrete specimen under tension, $k = 1.05311 \times 10^6$ and $m = 7.88917$.

† The overall compression may result in crack-closing during deformations [4]. The friction between crack surfaces renders an anisotropic elastic moduli tensor which is not accounted for in equation (14).

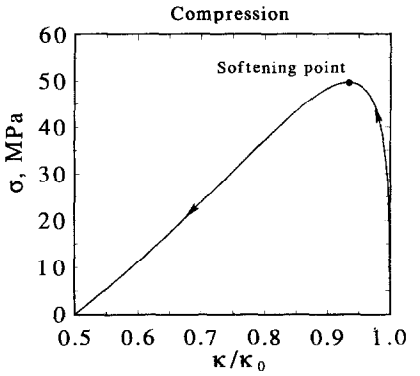

FIG. 7. Degradation of the overall thermal conductivity in the stress history. The concrete specimen under compression, $k = 1.51523 \times 10^8$ and $m = 9.52216$.

(b) *Internally pressurized cylinder—deformation induced inhomogeneity*

When load is applied to a structure, strain levels established at different locations depend on the way in which load is transmitted into the interior. For most problems with practical interest, load transmission is nonhomogeneous and the strain field thus established is consequently nonhomogeneous. The nonhomogeneous strains induce a nonhomogeneous distribution of microcracks which, in turn, generate a nonhomogeneous pattern for the degradation of overall thermal conductivity. As a quantitative example for illustrating this phenomenon, we consider an internally pressurized cylinder fixed along its outer surface as shown in Fig. 8. When the internal pressure P gradually increases, we study the evolution pattern of the overall thermal conductivity in the cylinder. The overall thermal conductivity represented by equation (4) has been implemented in the finite element algorithm developed by Tzou and Chen [5] to study the degradation load- and energy-bearing capacities as an entirety. The finite element approach employs an incremental algorithm to update the microcrack damage, and hence the overall thermal conductivity and elastic moduli, in the strain history. It employs nonlinear, isoparametric elements allowing for cubically-varying displacements inside each element. We use a total of 16 Gaussian points of integration in every element to capture the variation of the microcrack density inside the element. The required numerical accuracy can thus be achieved by the use of the least number of elements. The local and global Euclidean Error norms, respectively, are limited to 10^{-6} and 10^{-5}. Numerical iterations are proceeded until these threshold values are obtained. Eight elements are used to discretize the first-quadrant segment presenting axis-symmetry. Other details and results for the nonlinear stress analysis are provided in ref. [5] and will not be repeated here.

Based on the strain field thus calculated, the way to calculate the overall thermal conductivity remains the same. When the applied internal pressure increases from zero to 560 MPa, Fig. 9 shows the progressive degradation of the overall thermal conductivity in the cylinder at three intermediate stages with $P = 500$, 530, and 560 MPa. The case with $P = 500$ MPa is the onset for microcrack activation below which only a minor change in the thermal conductivity is observed. Different symbols on the curves represent typical nodal values obtained from the finite element analysis. The overall thermal conductivity, as expected, decreases when the internal pressure increases. At a given value of P, the inner surface subjecting to load and the outer surface being geometrically fixed possess larger volumetric strains. As a result, the microcrack damage and hence the degradation of overall thermal conductivity are thereby more pronounced. Note also that the thermal conductivity degrades to half of its intact value at the loaded inner surface when P reaches 560 MPa. This is the ultimate value of κ/κ_0 (1/2) and all the elastic moduli reduce to zero since $C_{ij} = 9/16$.

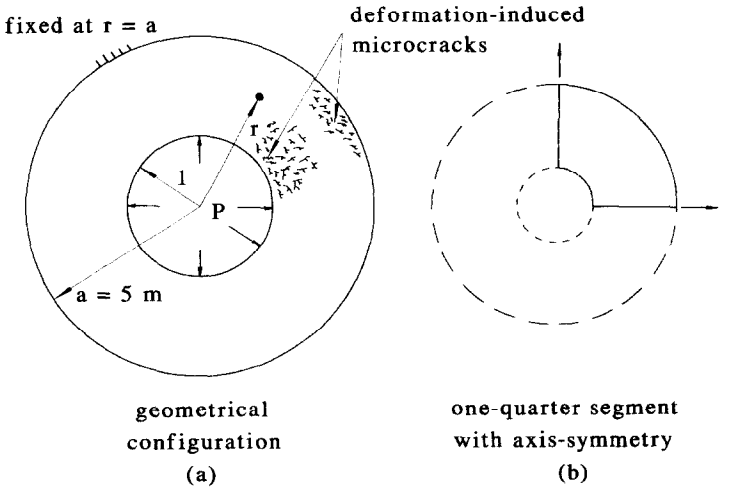

FIG. 8. (a) An internally pressurized cylinder fixed at the outer surface with $a = 5$ m and (b) one-quarter segment reflecting the axis-symmetry.

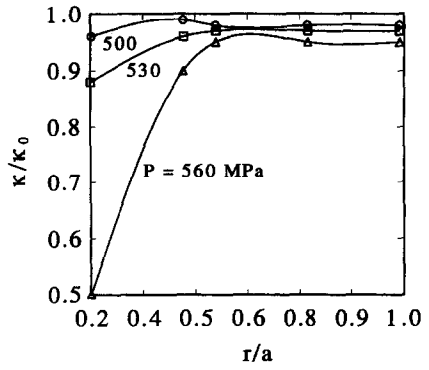

FIG. 9. Nonhomogeneous distributions of the overall thermal conductivity in the pressurized cylinder. Evolution patterns of κ/κ_0 at $P = 500$, 530 and 560 MPa.

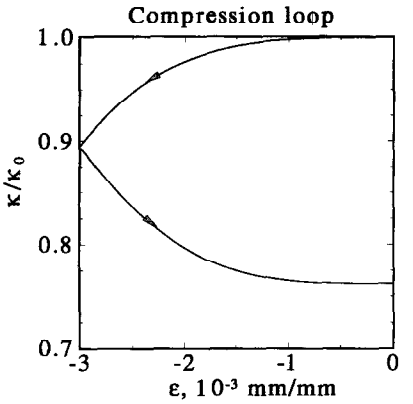

FIG. 10. Degradation history and permanent set of the overall thermal conductivity in a compression loop of strain: 0–-3.0×10^{-3}–0 mm mm^{-1}, $\nu_0 = 0.24$, $k = 1.51523\times10^8$ and $m = 9.52216$.

(c) *Path dependency*

The path dependency is a direct consequence of irreversibility in microcracking. It means that the microcrack density, and hence the overall thermal conductivity, depend not only on the load exerted on the cracked medium but also on the way in which such a load is applied. We shall illustrate this special feature by considering, respectively, a tensile and a compressive strain-loop imposed on a cracked specimen. An incremental analysis is needed for studying the path-dependency in a strain history. To this end, equations (4), (10) and (11) are expressed in their incremental forms:

$$\Delta C_d = \frac{27(9+32C_d\nu_0)\Delta D}{16(27-54D\nu_0+27\nu_0^2-192C_d\nu_0^2+256C_d^2\nu_0^2)} \tag{15}$$

$$\Delta D = k(m-6)\varepsilon^{m-7}(\Delta\varepsilon) \tag{16}$$

$$\frac{\Delta\kappa}{\kappa_0} = -\tfrac{8}{9}\Delta C_d. \tag{17}$$

The onset of microcrack damage determines the initial strain ε. The microcrack density parameter C_d and damage D at this strain level are then calculated, respectively, by equations (10) and (11). Based on these initial values, equations (15)–(17) are used to calculate the incremental changes of ΔD, ΔC_d, and $\Delta\kappa/\kappa_0$ in response to the incremental strain $\Delta\varepsilon$ imposed on the cracked specimen. The loading path determines the strain increment $\Delta\varepsilon$. For a series of $\Delta\varepsilon_i$, $i = 1, 2, \ldots, N$, decomposing a specified path of loading, the incremental changes calculated from (15)–(17) are constantly cumulated to the previous values. Mathematically,

$$\varepsilon^{(i)} = \varepsilon^{(i-1)} + (\Delta\varepsilon)^{(i)}, \quad D^{(i)} = D^{(i-1)} + (\Delta D)^{(i)},$$

and

$$C_d^{(i)} = C_d^{(i-1)} + (\Delta C_d)^{(i)},$$

$$\left(\frac{\kappa}{\kappa_0}\right)^{(i)} = \left(\frac{\kappa}{\kappa_0}\right)^{(i-1)} + \left(\frac{\Delta\kappa}{\kappa_0}\right)^{(i)} \tag{18}$$

with i being the number of increments in the loading history. To demonstrate this procedure which is necessary for numerical analysis, a cracked specimen subjected to a compression loop is considered. The intact Poisson's ratio is taken as 0.24 for unconfined concretes. The specimen is first strain-loaded to -3×10^{-3} mm mm^{-1} and then unloaded back to the origin. Since the entire process occurs in compression, the values of k and m under compression in equation (11) are used. Although the net strain at the final state is zero in this loop, the microcrack damage, and hence the overall thermal conductivity develops a permanent set. The result is shown by Fig. 10. Two hundred (200) increments are used for decomposing each strain-path. In compression from zero to -3×10^{-3} mm mm^{-1}, the overall thermal conductivity gradually degrades to approximately 90% of its intact value ($\kappa/\kappa_0 \simeq 0.9$). In the reversal path from -3×10^{-3} mm mm^{-1} to zero, however, the microcrack density continuously evolves and the overall thermal conductivity degrades all the way to 78% of its intact value ($\kappa/\kappa_0 \simeq 0.78$). Also, larger degradation for κ/κ_0 is developed in the reversal path. Figure 11 shows the

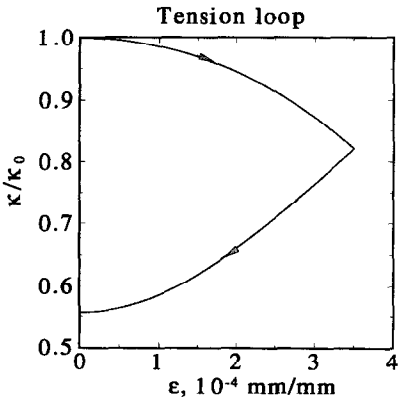

FIG. 11. Degradation history and permanent set of the overall thermal conductivity in a tension loop of strain: 0–3.5×10^{-4}–0 mm mm^{-1}, $\nu_0 = 0.24$, $k = 1.05311\times10^6$ and $m = 7.88917$.

result under tension. The cracked specimen in this case is loaded to 3.5×10^{-4} mm mm^{-1} and then unloaded back to the origin. The values of k and m under tension are used instead since the entire process occurs in tension. Again, the net strain imposed on the specimen is zero in this tension loop. Similar behavior is observed but a larger permanent set, namely $\kappa/\kappa_0 \simeq 0.56$, is developed at the end of the cycle. As explained in Figs. 4 and 5, this is due to weaker resistance to microcracking under tensile conditions.

CONCLUSION

Degradation of the overall thermal conductivity induced by microcracks has been analyzed in this paper. The micro-mechanical model established by Budiansky and O'Connell (for the elastic moduli) has been bridged to that established by Tzou (for the overall thermal conductivity) via the damage measure which evolves in the strain history. When strain is involved in the degradation process of the overall thermal conductivity, the effect of microcracking on the mechanical behavior has been accommodated for the sake of consistency. As a result, larger degradation has been found in the post-peak softening regime of the stress–strain curve. While deformation-induced material inhomogeneity for the overall thermal conductivity is demonstrated by a thick-wall cylinder subjected to an internal pressure, the path-dependency is demonstrated by a cracked specimen under tension- and compression-loops. The thermo–mechanical properties of an unconfined concrete specimen have been used to demonstrate this special behavior.

It has been found that as the crack density parameter reaches its ultimate value of 9/16, the load-bearing capacity of the continuum volume is totally lost as reflected by zero values of all the elastic moduli. The overall thermal conductivity, however, still has a residual value being one-half of its intact value at this critical instant. Physically, we have shown that the energy-bearing capacity degrades at a *slower* rate than the load-bearing capacity when microcrack damage evolves in the strain history. This is understood because heat conduction in solids relies not only on the effective surface area carrying the thermal energy, but also on the electron–phonon collisions in the process. Also, different degradation patterns of the overall thermal conductivity occur under tension and compression. Tension induces a larger degradation of the overall thermal conductivity which is a similar behavior to the elastic moduli.

Dependency on the loading path is a special feature for this type of problem. Under a specified final load, the microcrack density and hence the overall thermal conductivity may develop different permanent sets should the path of loading vary. The strain paths considered in Figs. 10 and 11 are designed for illustrating this important behavior in the simplest manner. It provides a fundamental understanding for problems in fatigue where both tension and compression may co-exist in loading cycles. When microcracks evolve in the strain history, indeed, the degradation history of the overall thermal conductivity becomes extemely complicated. The non-local spreading of the process zone from the surface of an internally pressurized cylinder and the path-dependency of the overall thermal conductivity, for example, are simply direct results of microcrack evolution. They are salient features in the present model which cannot be depicted by traditional approaches assuming elasticity for deformation.

Lastly, the 'overall' concept depends on the physical domain in averaging. For cracked solids with a fixed microcrack density, the overall thermal conductivity may be taken over the entire body. When strain and hence the microcracks evolve in a strain history, on the other hand, the physical domain for the *overall* thermal conductivity should be reduced to a substructural level to reflect the nonhomogeneous distributions of microcracks. The example of an internally pressurized cylinder given in this paper reflects this concept well.

REFERENCES

1. B. Budiansky, On the elastic moduli of some heterogeneous materials, *J. Mech. Phys. Solids* **13,** 223–227 (1965).
2. B. Budiansky, Thermal and thermoelastic properties of isotropic composites, *J. Compos. Mater.* **4,** 286–295 (1970).
3. B. Budiansky and R. J. O'Connell, Elastic moduli of a cracked solid, *Int. J. Solids Structures* **12,** 81–97 (1976).
4. F. G. Yost and D. Y. Tzou, Inhomogeneous grain growth due to shear, *Modeling of Coarsening and Grain Growth*, presented at the 1992 TMS Fall Meeting, Physical Metallurgy Committee, Naval Research Laboratory.
5. D. Y. Tzou and E. P. Chen, Mesocrack damage induced by a macrocrack in heterogeneous material, *Engng Fracture Mech.* **39,** 347–358 (1991).
6. H. Horii and S. Nemat-Nasser, Overall moduli of solids with microcracks: load-induced anisotropy, *J. Mech. Phys. Solids* **31,** 155–171 (1983).
7. D. P. H. Hasselman, Effect of cracks on thermal conductivity, *J. Compos. Mater.* **17,** 403–407 (1978).
8. A. Hoenig, Thermal conductivities of a cracked solid, *J. Compos. Mater.* **12,** 231–237 (1983).
9. D. Y. Tzou, A universal model for the overall thermal conductivity of porous media, *J. Compos. Mater.* **25,** 1064–1084 (1991).
10. D. Y. Tzou, The effect of internal heat transfer in cavities on the overall thermal conductivity, *Int. J. Heat Mass Transfer* **34,** 1839–1846 (1991).
11. A. Eucken, Thermal conductivity of ceramic refractory materials; calculation from thermal conductivity of constituents, *Forsch. Geb. Ing. Wes.*, B3, Forschungsheft No. 353, 16 (1972). *Ceramic Abstr.* **11,** 576 (1932); **12,** 231 (1933).
12. S. A. El-Fekey, Y. M. El-Mamoon and M. N. A. El-Hakim, Mathematical analysis of the dependence of thermal conductivity on porosity, *Power Metallurgy Int.* **37,** 80–81 (1978).
13. J. Francl and W. D. Kingery, Thermal conductivity: IX, Experimental investigation of effect of porosity in

thermal conductivity, *J. Am. Ceramic Soc.* **37,** 99–107 (1954).
14. J. S. Agapiou and M. F. Devries, An experimental determination of the thermal conductivity of a 304L stainless steel powder metallurgy material, *ASME J. Heat Transfer* **111,** 281–286 (1989).
15. D. Krajcinovic, Continuum damage mechanics, *ASME Appl. Mech. Rev.* **37,** 1–6 (1984).
16. D. Krajcinovic, Damage mechanics, *J. Mech. Mater.* **8,** 117–197 (1989).
17. D. Y. Tzou, The effect of thermal conductivity on the singular behavior of the near-tip temperature gradient, *ASME J. Heat Transfer* **113,** 806–813 (1991).
18. D. Y. Tzou, The singular behavior of the temperature gradient in the vicinity of a macrocrack tip, *Int. J. Heat Mass Transfer* **33,** 2625–2630 (1991).
19. L. M. Taylor, E. P. Chen and J. S. Kuszmaul. Microcrack-induced damage accumulation in brittle rock under dynamic loading, *Comput. Methods Appl. Mech. Engng* **55,** 301–320 (1986).